ARTICLE IN PRESS

International Journal of Plasticity xxx (xxxx) xxx

Contents lists available at ScienceDirect

International Journal of Plasticity

journal homepage: www.elsevier.com/locate/ijplas

A novel elastic–plastic damage model for rock materials considering micro-structural degradation due to cyclic fatigue

J. Zhang [a], W.Y. Liu [a], Q.Z. Zhu [a], J.F. Shao [a,b,*]

[a] Key Laboratory of Ministry of Education for Geomechanics and Embankment Engineering, Hohai University, Nanjing, China
[b] Univ. Lille, CNRS, Centrale Lille, UMR 9013 - LaMcube - Laboratoire de mécanique multiphysique et multiéchelle, Lille, F-59000, France

ARTICLE INFO

Keywords:
Rock materials
Cyclic lading
Fatigue damage
Constitutive model
Micro-structure

ABSTRACT

In this work, a novel constitutive model is developed to describe the mechanical behavior of rock like materials subjected to cyclic loading. The fatigue damage is physically related to the progressive micro-structural degradation which is described by a convolutional law. The number of cycles is considered as an equivalent time in the description of creep deformation. The fatigue damage evolution is further coupled with the plastic deformation. The evolution of fatigue damage is driven by the applied stress amplitude and number of cycles through the coupling with the accumulated plastic deformation. The proposed model is able to describe the mechanical responses of materials under both monotonic and cyclic loading conditions. The mechanical responses of two representative rocks, argillaceous quartz siltstone and salt rock, are investigated by the proposed model. All main behavior features of these materials are well captured by the proposed model.

1. Introduction

In the operation stage of rock engineering constructions, the mechanical properties of rock mass under cyclic loading is one of the important factors affecting the long-term stability. Discovering the fatigue damage characteristics and evolution law is essential to correctly understand the failure mechanism of rock mass, and then properly evaluate the long-term stability of rock structures. The research on failure mechanism of rocks under cyclic loading has been for long time one of the frontier subjects in rock mechanics and engineering (Chen et al., 2020; Xu et al., 2022; Zhang et al., 2022b). Actually, experimental studies have clearly demonstrated that the failure strength under monotonic loading cannot guarantee the long-term stability and safety of structures (Kobayashi et al., 1992; Zhang et al., 2017b), and the durability is very sensitive to the stress level under cyclic loads (Liu and He, 2012).

Under cyclic loading with variable stress amplitude, two typical types of fracture may occur even below the ultimate monotonic failure strength: ratcheting or incremental collapse due to an excessive deformation via accumulation of plastic strain; or accommodation or fatigue by reaching a stabilized cycle of plastic strains, although the increment of deformation is small in each cycle (Zhang et al., 2019, 2022a, 2017a). In another example, after a finite number of cycles, the progressive mechanical response becomes equivalently elastic, and the total dissipation is bounded. One reaches a shakedown state (Spiliopoulos and Panagiotou, 2017; Surmiri et al., 2018), which is characterized by the shakedown limit, beyond which the material will fail due to fatigue. However, the shakedown behavior of rock like materials is rarely observed compared with metals. This is due to the crack initiation and propagation in each loading cycle once the applied load exceeds the elastic limit. As a consequence, the material will eventually reach the failure state by fatigue or ratcheting (Wang et al., 2021; Han et al., 2020; Miao et al., 2021b). Therefore, the cumulative

* Corresponding author at: Univ. Lille, CNRS, Centrale Lille, UMR 9013 - LaMcube - Laboratoire de mécanique multiphysique et multiéchelle, Lille, F-59000, France.
E-mail address: jian-fu.shao@polytech-lille.fr (J.F. Shao).

https://doi.org/10.1016/j.ijplas.2022.103496
Received 21 September 2022; Received in revised form 14 November 2022
Available online 12 December 2022

Please cite this article as: J. Zhang, *International Journal of Plasticity*, https://doi.org/10.1016/j.ijplas.2022.103496

inelastic deformation and evolution of micro-cracks are two crucial factors controlling the long-term failure of rock-like materials under cyclic loading.

To this end, various measurement methods have been proposed to quantify the micro-structural degradation and its consequences on macroscopic behavior. For instance, the acoustic emission signal (energy and count) is widely used to determine the evolution and localization of micro-cracks (Naderloo et al., 2019; Xue et al., 2020; Jian-po et al., 2015). In some studies, the acoustic emission is combined with the nuclear magnetic resonance to identify the porosity, uniaxial strength and dynamic fracture characteristics of brittle rocks before and after cyclic loading (Meng et al., 2018; Yang et al., 2022). In another study on rock salt subjected to multilevel cyclic loading, the acoustic emission monitoring and CT scanning was used (Zhao et al., 2022). It is found that the cyclic damage evolution exhibits a two-phase pattern, the damage part during the accelerated deformation phase represents a major part of the total induced damage.

In the recent decades, important efforts have been concentrated on elastoplastic damage modeling for rock like materials. Theoretical frameworks of isotropic damage models have been developed by various authors (Dragon and Mroz, 1979; Frantziskonis and Desai, 1987; Shao et al., 2006; Wu et al., 2006) just to mention a few, in which the induced damage is characterized by scalar damage parameters. Considering the effects of anisotropic distribution of microcracks and microvoid, anisotropic damage models have also been formulated with or without the plastic coupling for quasi-brittle materials (Abu-Lebdeh and Voyiadjis, 1993; Luccioni and Rougier, 2005; Jason et al., 2006), by adopting the micro-plane theory (Carol and Bazant, 1997), discrete thermodynamics formulation (Zhu et al., 2010) and homogenization techniques (François and Dascalu, 2010; Zhu and Shao, 2015). In particular, Voyiadjis et al. (2008, 2022) have introduced second-order damage tensors to describe the anisotropic behaviors by taking account of the different tensile and compressive damage characteristics. Using the 3D digital image technique with finite element method, Mazzucco et al. (2020a,b) have reconstructed the concrete close to failure and modeling the material at mesoscale. A It is referred to Park et al. (2022) for the detailed introduction of plastic damage model of concrete.

Concerning the constitutive modeling of cyclic deformation and failure of rock materials, numerous contributions (Lee and Fenves, 1998; Cerfontaine et al., 2017; Zhou et al., 2020) have firstly been made in the elasto-plastic framework. Besides, the internal state variables are employed to describe the fatigue properties (Wang et al., 2013; Liu and Dai, 2018; Zhou et al., 2017). Considering the deformation and failure of rocks are generally accompanied with energy dissipation, constitutive models from the perspective of energy (Ye and Wang, 2001; Song et al., 2018; Liu et al., 2016) are constructed by combining the energy dissipation and damage evolution. At last, discrete element-based approaches (Liu et al., 2017; Yu et al., 2021) are also proposed for rock and concrete. Particularly, by introducing induced damage process, different types of empirical laws have been proposed to describe the fatigue damage. For instance, a linear–exponential formula is proposed in Xiao et al. (2011), which improves the inverted-S damage model (Xiao et al., 2009). Besides, a number of factors have been taken into account in different models, such as loading frequency (Wang et al., 2016; Ren et al., 2022), loading rate (Moreo et al., 2007), energy dissipation (Miao et al., 2021a) and the micro-structure (Sandoval et al., 2020; Baktheer et al., 2021). By introducing the concept of compaction coefficient and using the strain equivalence principle, an amended damage constitutive model was established in Liu et al. (2016). Recently, by the identification of three stages of the deformation of salt rock in cyclic tests, an exponential cumulative damage model was provided in He et al. (2019) to predict its lifetime. But the existence of a steady stage of deformation and the underlying mechanisms of fatigue failure of rock like materials under cyclic loading have not been systematically investigated in most previous studies. Considering that the accumulated deformation is usually the most important information needed to be monitored in engineering, the interest of this study is concentrated on the accumulated deformation at the end of each cycle. And a mathematical function is needed to accurately describe the progressive fatigue-induced damage.

Consequently, the present work is devoted to modeling of deformation and failure of rock materials subjected to both monotonic and cyclic loads. The basic mechanical behavior of materials is described by an elastic–plastic damage model (Liu et al., 2011; Xu and Lu, 2013). The cumulative macroscopic strains during loading cycles are considered as the consequence of micro-structural degradation, mainly the nucleation and propagation of micro-cracks (Toro et al., 2016; Cao et al., 2022). Inspired by the previous studies devoted to the description of time-dependent creep deformation of rocks (Shao et al., 2003; Pietruszczak et al., 2004; Zhao et al., 2018), a new evolution law of fatigue damage is proposed by considering the number of cycles as an equivalent time scale. As a basic difference with most previous models, the evolution of damage is driven by the deviation from a self-equilibrium state. In this way, both short-term and long-term mechanical responses can be described by a unified model. However, the majority of cyclic tests on rock materials performed so far are under compressive stresses. Very few data are available for the tensile cyclic loading tests. Therefore, for the sake of simplicity, only one scalar damage variable is adopted to represent material degradation due to cyclic loading. The difference between tensile and compressive cyclic damage will be investigated in future study.

This paper is organized as follows. A convolutional formulation is firstly introduced in Section 2 for the description of fatigue damage evolution under cyclic loads. The effects of load amplitude and cycle number are taken into account. Then, an elastic–plastic model is formulated by incorporating the fatigue-induced damage in Section 3. In Section 4, the proposed model is implemented by the use of a non-linear explicit integral algorithm. It is further applied to investigate mechanical responses of two rocks, argillaceous quartz siltstone and salt rock, in monotonic and cyclic tests. The evolution of macroscopic elastic properties, failure modes and fatigue lifetime of tested materials are discussed. Some concluding remarks are provided in the last section.

2. Typical mechanical responses of rock materials under cyclic loading and description of fatigue induced damage

In this section, we shall first briefly recall the typical mechanical behavior of rocks under cyclic loading in terms of cumulative deformation. Based on this, a convolutional law is established to describe the cumulative deformation by incorporating the micro-structural evolution.

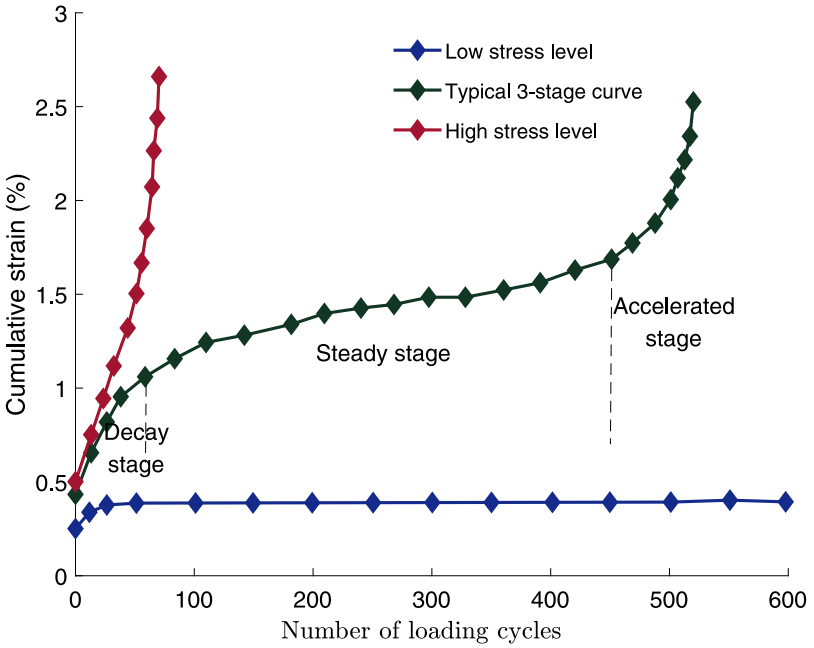

Fig. 1. Three typical evolution curves of cumulative strain of rock materials during cyclic loading with a constant amplitude but different upper limit stress level. (For interpretation of the references to color in this figure legend, the reader is referred to the web version of this article.)

2.1. Typical cumulative deformation curves of rock materials in cyclic loading

According to the experimental studies on the mechanical properties of rock-like materials under cyclic loading (Fuenkajorn and Phueakphum, 2010; Wang et al., 2021), the fatigue behavior is affected by several factors, such as load amplitude, upper and lower stress levels, loading frequency and waveform. The elastic part of deformation can be recovered during the unloading process in each cycle, but the inelastic part is irreversible and progressively accumulated until the failure of material. Consequently, the evolution form of accumulated strain is an essential indicator of the mechanical property degradation of material with the increase of loading cycles. Moreover, the evolution of macroscopic accumulated strain is inherently related to the change of micro-structure. Therefore, it is convenient to characterize the progressive degradation process of materials due to fatigue in relation with the accumulated irreversible deformation.

Three typical evolution curves of cumulative strain of rocks during cyclic loading with a constant load amplitude are presented in Fig. 1. The total strain is recorded in each loading cycle at the peak of strain–stress loop. It is obvious that the accumulated strain evolution curves are very similar to those of the creep deformation in rocks (Wang et al., 2022; Huang et al., 2015). In particular, the fatigue induced deformation is dependent on the applied stress level. For an appropriate load amplitude, one gets a typical 3-stage curve of cumulative strain with an inverted S-shape (green line in Fig. 1). More precisely, the cumulative strain exhibits a rapid increase at the beginning of cyclic loading. After a certain number of cycles, the evolution rate gradually decreases and becomes constant during the second stage. In the third stage, an acceleration of increase rate is obtained until the failure due to an excessive accumulation of inelastic strain. Therefore, the whole evolution curve can be reasonably divided into three distinct stages: decay stage, steady stage and accelerated stage (Wang et al., 2021). This is similar to the three stages of creep deformation, namely primary, stationary and accelerated creep.

Other types of evolution can be seen as a particular case when the second or third stage vanishes respectively. For example, if the upper stress limit is high or the material exhibits a strong brittle property, the steady stage could be very short or even does not exist, rapidly leading to the failure after very few number of cycles (red line in Fig. 1). On the contrary, if the upper cyclic stress is small, the cumulative strain stabilizes after the initial stage (blue line in Fig. 1) and do not exhibit the accelerated stage even for a high number of cycles. In this situation, the fatigue failure will not occur at least for a given period. This case can be considered in the shakedown or high-cycle fatigue domain as mentioned in the introduction. Noticing that the loading frequency (retention time of load) and the waveform are not taken into account in the present study.

According to micro-CT scanning images of rock specimens subjected to monotonic and cyclic loads (Yang et al., 2015), crack flats are featured complex with more micro-cracks under cyclic load than that under monotonic load. As shown in Fig. 2, both the crack region and aperture range in cyclically failed specimens surpass those in monotonic way, which is considered as the consequence micro-structural degradation. That indicates us to introduce a damage variable to describe the progressive degradation due to fatigue.

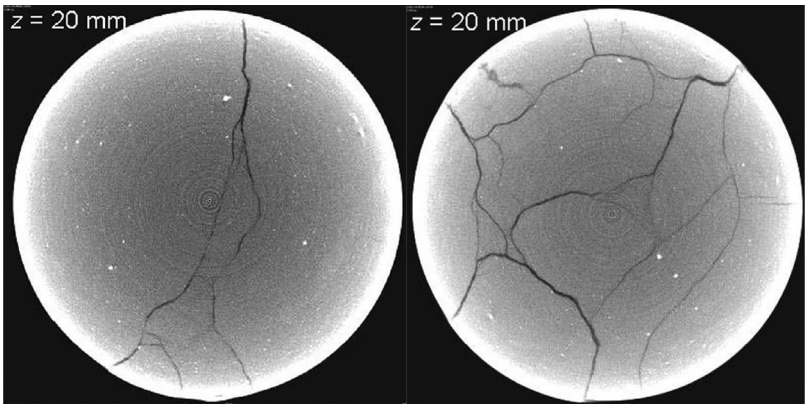

Fig. 2. Micro-CT scanning images of rock specimens under monotonic load (left) and cyclic load (right) by Yang et al. (2015).

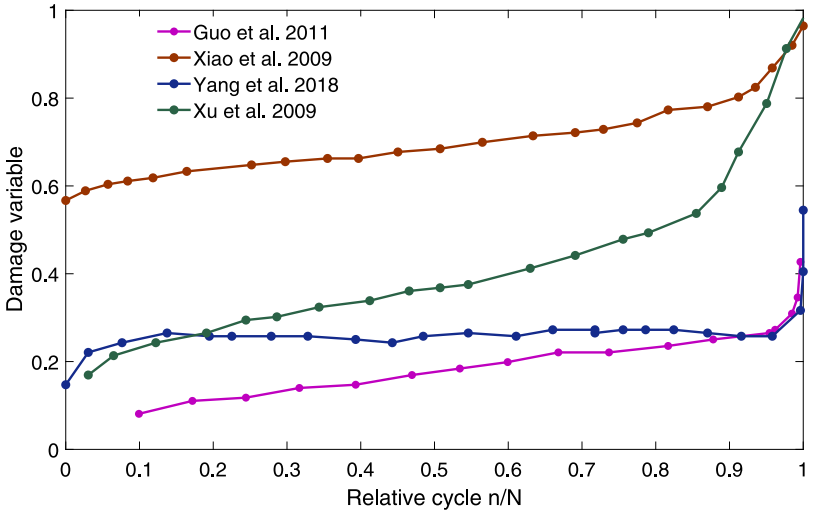

Fig. 3. Evolution curves of fatigue damage variable for different rocks under cyclic loads.

The accumulated damage due to fatigue have also been investigated experimentally by scholars (Xiao et al., 2009; Xu et al., 2009; Guo et al., 2011; Yang et al., 2018) for different types of rocks. The damage evolution are plotted in Fig. 3, in which an inverted-S shaped curve with three phases can be observed. In addition, according with the development of fatigue deformation in Fig. 1, it is reasonable to construct a fatigue model by considering the progressively accumulated damage variable.

2.2. Description of fatigue induced material degradation

Based on the experimental evidence presented above, the emphasis is here put on the evolution of cumulative inelastic strains. It is assumed that two dissipation mechanisms should be taken into account, plastic deformation and damage due to growth of micro-cracks. The plastic deformation can be described by a classical plastic model, which is presented later. The description of fatigue damage evolution due to cyclic loading is the key issue. As mentioned above, a stationary state potentially exists, illustrated by the steady stage in Fig. 1, during cyclic loading. This one is related to the material property and loading history. A deviation from this stationary state leads to an accelerated accumulation of total deformation and fatigue failure. Like in the classical continuum damage mechanics, a scalar internal variable ω is introduced to represent the current state of material degradation caused by cyclic loading. Based on the previous study devoted to creep deformation due to micro-structural degradation (Pietruszczak et al., 2004), the evolution rate is described by the following equilibrium equation:

$$\dot{\omega} = \gamma\,(\bar{\omega} - \omega) \tag{1}$$

in which $\dot{\omega}$ represents the damage evolution rate and $\bar{\omega} \geq \omega$ denotes the stationary state associated with the equilibrium of micro-structural degradation. The parameter γ controls the kinetics of damage evolution. It is obvious that when $\omega \leq \bar{\omega}$, there is an increase

of micro-structural degradation. Its kinetics is driven by the distance between the current state and the equilibrium one ($\bar{\omega} - \omega$). When the current state approaches the stationary one, $\omega \to \bar{\omega}$, the damage evolution decreases and eventually vanishes.

Considering the similarity with the description of creep deformation, the number of cycles n is here considered as an equivalent time variable. Thus both ω and $\bar{\omega}$ are function of n. Therefore, the damage evolution law can be rewritten as follows by using the Laplace transform:

$$\mathcal{L}(\omega) = \mathcal{L}(\gamma e^{-\gamma n})\, \mathcal{L}(\bar{\omega}) \tag{2}$$

It is now assumed that at the initial state, there is no damage. One has $\omega(0) = 0$ and $\omega \in [0, \bar{\omega}]$. By applying the convolution theorem to Eq. (2), the fatigue damage of material after N cycles can be obtained by the integral function:

$$\omega = \int_0^N \bar{\omega}(n)\gamma e^{-\gamma(N-n)} \mathrm{d}n \tag{3}$$

The exponential term $e^{-\gamma(N-n)}$ defines a memory function, which allows considering the dependency of the fatigue damage on the number of loading cycles. For the reason of convenience, the detailed derivation of the integral function (3) is given in Appendix A.

It is worth noticing that during the cyclic loading, these is an accumulation of inelastic strain, which depends on the number of cycles. Therefore, the micro-structural damage parameter ω, its stationary value $\bar{\omega}$ and evolution rate are all functions of accumulated inelastic strain. In particular, the evolution of the stationary damage parameter $\bar{\omega}$ with the accumulated inelastic strain is a key relation to be defined. This issue will be discussed in the next section.

3. Formulation of elastoplastic model with fatigue-damage

In the current section, a novel constitutive model is formulated for modeling the mechanical behavior of rock-like materials under both monotonic and cyclic loads by incorporating the micro-structural degradation. Starting from an elastoplastic model for the description of fundamental mechanical behavior under monotonic loads, the formulation is extended to cyclic cases by introducing the fatigue damage.

3.1. Basic elastoplastic model

It is assumed that the basic mechanical behavior of rocks can be described by elastoplastic models. With the assumption of small strains, the total linear strain tensor ε_{ij} is decomposed into an elastic part ε_{ij}^e and a plastic part ε_{ij}^p, that is:

$$\varepsilon_{ij} = \varepsilon_{ij}^e + \varepsilon_{ij}^p \tag{4}$$

The elastoplastic strain–stress relations can be expressed in the following general form:

$$\sigma_{ij} = C_{ijkl}^0 \varepsilon_{kl}^e = C_{ijkl}^0 \left(\varepsilon_{kl} - \varepsilon_{kl}^p\right) \tag{5}$$

where C_{ijkl}^0 are the components of the fourth-order elastic stiffness tensor of intact materials. σ_{ij} denotes the Cauchy stress tensor. By adopting the assumption of isotropic materials, the elastic tensor is a function of the shear modulus μ_0 and bulk modulus k_0, such as:

$$C_{ijkl}^0 = 3k_0 J_{ijkl} + 2\mu_0 K_{ijkl} \tag{6}$$

J_{ijkl} and K_{ijkl} are the components of fourth-order hydrostatic and deviatoric projectors, respectively. In the case of constant elastic stiffness tensor, the elastoplastic stress–strain relation can be given in the incremental form:

$$\mathrm{d}\sigma_{ij} = C_{ijkl}^0 \left(\mathrm{d}\varepsilon_{kl} - \mathrm{d}\varepsilon_{kl}^p\right) \tag{7}$$

For the description of plastic strain, a yield function is first defined. For most frictional geological materials, the mechanical strength is strongly dependent on confining pressure which is represented by the mean stress in general loading conditions. The pressure dependency is described through the international frictional angle. Considering that the peak strength will not be reached in laboratory cyclic tests, we adopt the following nonlinear plastic yield function and hardening rule, which have been applied to describe the mechanical behaviors of quasi-brittle materials in compression tests (Chiarelli, 2000; Shao et al., 2003; Qu et al., 2019):

$$f(\sigma_{ij}, \alpha_p) = \sigma_{eq}^2 + A_0 \alpha_p \left(\sigma_m - C\right) \leq 0 \tag{8}$$

σ_m denotes the mean stress, and σ_{eq} is the deviatoric stress, defined as:

$$\sigma_m = \frac{1}{3}\sigma_{kk}, \quad \sigma_{eq} = \sqrt{\frac{3}{2}(K_{ijkl}\sigma_{kl})(K_{ijkl}\sigma_{kl})} \tag{9}$$

The parameters A and C are respectively related to the maximum frictional coefficient and the cohesion of material at the failure state. The function α_p denotes the activation ratio of the frictional coefficient A. Besides, according to the experimental investigation and theoretical modeling of hard claystone (Chiarelli, 2000), it is assumed that materials exhibit an isotropic hardening law, leading

to an increase of the frictional coefficient activation ratio α_p from its initial value α_p^0 to 1. The following hardening rule is adopted in hyperbolic form:

$$\alpha_p(\gamma^p) = \alpha_p^0 - \left(1 - \alpha_p^0\right) \frac{\gamma^p}{\gamma^p + B} \tag{10}$$

The plastic hardening rate is controlled by the parameter B. Consequently, the proposed fatigue damage model can capture the main mechanical property in monotonic case before peak strength and be expressed in a concise form. γ^p is the equivalent plastic shear strain and defined by:

$$\gamma^p = \int \sqrt{\frac{2}{3}(K_{ijkl}\mathrm{d}\varepsilon_{kl}^p)(K_{ijkl}\mathrm{d}\varepsilon_{kl}^p)} \tag{11}$$

On the other hand, for most geological materials, a non-associated flow rule is usually necessary due to complex plastic deformation kinetics, for instance the transition from volumetric compressibility to dilatancy (Pietruszczak et al., 1988). For this purpose, the following plastic potential function is adopted:

$$g(\sigma_{ij}) = \sigma_{eq} + A_0\eta\left(\sigma_m - C\right)\ln\left(\sigma_m - C\right) = 0 \tag{12}$$

The parameter η controls the sign of plastic volumetric strain. One gets a plastic contractance for $\alpha_p < \eta$ and a dilatancy for $\alpha_p > \eta$. The contractance–dilatancy transition is defined by $f_{cd} = \sigma_{eq} + A\eta\left(\sigma_m - C\right) = 0$. The plastic strain increments are given by the flow rule:

$$\mathrm{d}\varepsilon_{ij}^p = \mathrm{d}\lambda\frac{\partial g}{\partial \sigma_{ij}} \tag{13}$$

$\mathrm{d}\lambda$ is the non-negative plastic multiplier, which is determined from the consistency condition.

3.2. Formulation of elastoplastic fatigue damage model

The basic elastoplastic model is now extended to cyclic loading by incorporating isotropic fatigue damage effects. Based on the previous experimental studies (Fuenkajorn and Phueakphum, 2010; Fan et al., 2016; Wang et al., 2021), the elastic properties and the failure strength of materials are both weakened by the fatigue induced damage. For isotropic materials, it is assumed that the bulk and shear modulus as well as the maximum frictional coefficient A are functions of the fatigue damage parameter ω. The following linear forms are adopted:

$$k(\omega) = (1 - \alpha_1\omega)k_0 \quad , \quad \mu(\omega) = (1 - \alpha_1\omega)\mu_0 \quad , \quad A(\omega) = (1 - \alpha_2\omega)A_0 \tag{14}$$

μ_0, μ_0 and A_0 are the values of elastic moduli and maximum frictional coefficient of intact materials. Two parameters α_1 and α_2 control their degradation rate due to fatigue damage.

The effective fourth-order elastic tensor has the following relation with the initial value: $C_{ijkl} = (1 - \alpha_1\omega)C_{ijkl}^0$. Accordingly, introducing the degradation of elastic parameters in to constitutive relations Eqs. (5) and (7), we obtain:

$$\begin{aligned} \sigma_{ij} &= \left(1 - \alpha_1\omega\right)C_{ijkl}^0\left(\varepsilon_{kl} - \varepsilon_{kl}^p\right) \\ \mathrm{d}\sigma_{ij} &= \left(1 - \alpha_1\omega\right)C_{ijkl}^0\left(\mathrm{d}\varepsilon_{kl} - \mathrm{d}\varepsilon_{kl}^p\right) - \alpha_1 C_{ijkl}^0\left(\varepsilon_{kl} - \varepsilon_{kl}^p\right)\mathrm{d}\omega \end{aligned} \tag{15}$$

C_{ijkl}^0 are the components of initial elastic stiffness tensor of intact materials. The plastic yield function and potential of damaged materials are also extended to the following forms coupling with the fatigue-induced damage:

$$f(\sigma_{ij}, \alpha_p, \omega) = \sigma_{eq}^2 + (1 - \alpha_2\omega)A_0\alpha_p\left(\sigma_m - C\right) \le 0 \tag{16}$$

$$g(\sigma_{ij}, \omega) = \sigma_{eq} + (1 - \alpha_2\omega)A_0\eta\left(\sigma_m - C\right)\ln\left(\sigma_m - C\right) = 0 \tag{17}$$

3.2.1. Application to strain-prescribed loading

The proposed elastoplastic fatigue damage model is applied to strain-prescribed loading conditions in view of its numerical implementation in computer codes for engineering applications. Considering the material degradation and plastic hardening, the plastic consistency condition is expressed as follows:

$$\mathrm{d}f = \frac{\partial f}{\partial \sigma_{ij}}\mathrm{d}\sigma_{ij} + \frac{\partial f}{\partial \alpha_p}\mathrm{d}\alpha_p + \frac{\partial f}{\partial \omega}\mathrm{d}\omega = 0 \tag{18}$$

The increment of fatigue damage is a function of cycle number:

$$\mathrm{d}\omega = \dot{\omega}\mathrm{d}n \tag{19}$$

Substituting the stress–strain relations (15), the plastic hardening law (10) and the plastic flow rule (13) for (18), one gets the plastic multiplier as follows:

$$\mathrm{d}\lambda = \frac{\left(1 - \alpha_1\omega\right)\frac{\partial f}{\partial \sigma_{ij}}C_{ijkl}^0\mathrm{d}\varepsilon_{kl} - \left(\alpha_1\frac{\partial f}{\partial \sigma_{ij}}C_{ijkl}^0\mathrm{d}\varepsilon_{kl}^e + \alpha_2 A_0\frac{\partial f}{\partial A}\right)\mathrm{d}\omega}{H_\varepsilon} \tag{20}$$

The related plastic hardening modulus H_ϵ is given by:

$$H_\epsilon = (1-\alpha_1\omega)\frac{\partial f}{\partial \sigma_{pq}} C^0_{pqrs}\frac{\partial g}{\partial \sigma_{rs}} - \frac{\partial f}{\partial \alpha_p}\frac{\partial \alpha_p}{\partial \gamma^p}\frac{\partial g}{\partial \sigma_{eq}} \tag{21}$$

Putting the expression of plastic multiplier (20) into the strain–stress relation (15), the general incremental form of the constitutive equations can be obtained for strain-prescribed condition:

$$\mathrm{d}\sigma_{ij} = C^{tan}_{ijkl}\mathrm{d}\varepsilon_{kl} + \Pi_{ij}\dot{\omega}\mathrm{d}n \tag{22}$$

C^{tan}_{ijkl} denotes the fourth-order tangent stiffness tensor, given by:

$$C^{tan}_{ijkl} = (1-\alpha_1\omega)\left(C^0_{ijkl} - \frac{(1-\alpha_1\omega)}{H_\epsilon} C^0_{ijpq}\frac{\partial g}{\partial \sigma_{pq}}\frac{\partial f}{\partial \sigma_{rs}} C^0_{rskl}\right) \tag{23}$$

The second-order tensor Π_{ij} representing the increment of stress due to cyclic loading history takes the following form:

$$\Pi_{ij} = \frac{(1-\alpha_1\omega)}{H_\epsilon}\left(\alpha_1 C^0_{ijpq}\frac{\partial g}{\partial \sigma_{pq}}\frac{\partial f}{\partial \sigma_{rs}} C^0_{rskl}\varepsilon^e_{kl} + \alpha_2 A_0\frac{f}{A_0} C^0_{ijkl}\frac{\partial g}{\partial \sigma_{kl}}\right) - \alpha_1 C^0_{ijkl}\varepsilon^e_{kl} \tag{24}$$

It is obvious that the stress increment in (22) is composed of two terms. The first one depends on the strain increment and corresponds to the response of an elastoplastic damaged material under monotonic loading ($\mathrm{d}n = 0$). The second term represents the stress change due to cyclic loading induced fatigue damage.

3.2.2. Application to stress-prescribed loading

For some specific cases, for instance simulation of laboratory tests, it is convenient to formulate the constitutive model for stress-prescribed loading conditions. For this purpose, the fourth-order elastic compliance tensor $D^0_{ijkl} = (C^0_{ijkl})^{-1}$ of intact materials is defined. Then, the elastic strain tensor can be determined by:

$$\varepsilon^e_{ij} = \frac{1}{1-\alpha_1\omega} D^0_{ijkl}\sigma_{kl} \tag{25}$$

Accordingly, the increment form of the elastic strain $\mathrm{d}\varepsilon^e_{ij}$ takes the following form:

$$\mathrm{d}\varepsilon^e_{ij} = \frac{1}{1-\alpha_1\omega} D^0_{ijkl}\mathrm{d}\sigma_{kl} + \frac{\alpha_1}{(1-\alpha_1\omega)^2} D^0_{ijkl}\sigma_{kl}\mathrm{d}\omega \tag{26}$$

Substituting the above Eq. (26) and the plastic flow rule (13) into the plastic consistency condition (18), one obtains the plastic multiplier:

$$\mathrm{d}\lambda = \frac{\frac{\partial f}{\partial \sigma_{ij}}\mathrm{d}\sigma_{kl} - \alpha_2 A_0\frac{\partial f}{\partial A}\mathrm{d}\omega}{H_\sigma} \tag{27}$$

where the plastic hardening modulus H_σ is given by:

$$H_\sigma = -\frac{\partial f}{\partial \alpha_p}\frac{\partial \alpha_p}{\partial \varepsilon^p_{eq}}\frac{\partial g}{\partial \sigma_{eq}} \tag{28}$$

By using the expressions of the plastic multiplier (27) and of the elastic strain increment (26), one gets the incremental form of strain–stress relations for elastoplastic damaged materials under stress-prescribed conditions:

$$\mathrm{d}\varepsilon_{ij} = D^{tan}_{ijkl}\mathrm{d}\sigma_{kl} + \Xi_{ij}\dot{\omega}\mathrm{d}n \tag{29}$$

D^{tan}_{ijkl} is the fourth-order tangent compliance tensor given by:

$$D^{tan}_{ijkl} = \frac{1}{1-\alpha_1\omega} D^0_{ijkl} + \frac{1}{H_\sigma}\frac{\partial g}{\partial \sigma_{ij}}\frac{\partial f}{\partial \sigma_{kl}} \tag{30}$$

The second-order tensor Ξ_{ij} defines the effect of fatigue damage and it is given by:

$$\Xi_{ij} = \frac{1}{(1-\alpha_1\omega)^2} D^0_{ijkl}\sigma_{kl} - \frac{\alpha_2}{H_\sigma} A_0\frac{\partial f}{\partial A}\frac{\partial g}{\partial \sigma_{ij}} \tag{31}$$

Similarly to the strain-prescribed loading, the strain increment under stress-prescribed loading is divided into two terms. The first one provides the strain due to stress variation in an elastoplastic damaged material under monotonic loading. The second term represents the strain variation induced by the evolution of fatigue damage during cyclic loading.

4. Model assessment

In this section, the proposed elastoplastic fatigue damage model is evaluated for typical rocks under both monotonic and cyclic loading conditions.

Table 1
Identified values of elastic–plastic parameters for argillaceous quartz siltstone.

E (MPa)	ν	A_0	C (MPa)	α_p^0	B	η
5200	0.27	62	13	0.027	0.0011	−0.0015

4.1. Numerical implementation of the proposed model

The proposed model is implemented in the framework of finite element method though the emphasis is put on the mechanical response of a material point (Gauss integration point). The whole loading history is divided into a number of steps. Starting from the initial conditions, it is assumed that the values of stresses, strains, generalized plastic strain and fatigue damage are all known at the beginning of each step. An increment of strains or cycle number is prescribed at each step. The solutions to determine are the corresponding stresses and accumulated strain due to loading cycles, by using the proposed constitutive relations.

However, differently with classical monotonic elastoplastic model, the evolution of fatigue damage is here described by the specific integral function (3). Similarly to monotonic loading, the total number of cycles N is also divided into a series of increments. For each increment of cycle number, a variation of fatigue damage is evaluated according to (3). Inspired by the study of creep deformation (Zhu et al., 2016a) and after a rigorous mathematical transformation presented in Appendix B, the following non-linear explicit integral algorithm is adopted:

$$\omega_n = \omega_{n-1} e^{-\gamma \mathrm{d}n} + \gamma \left(\frac{\bar{\omega}_n + \bar{\omega}_{n-1}}{2} \right) e^{-\frac{1}{2}\gamma \mathrm{d}n} \tag{32}$$

It is found that the current value of fatigue damage ω_n depends on the values of stationary damage variable at the current and previous steps, say $\bar{\omega}_n$ and $\bar{\omega}_{n-1}$. As mentioned above, the variation of $\bar{\omega}$ depends on the loading history, in particular plastic strains. Inspired by the time-dependent deformation modeling of brittle rocks (Zhu et al., 2016b), it is assumed that $\bar{\omega}$ is a function of the generalized plastic strain γ^p:

$$\bar{\omega} = C_1 \, \alpha_p \, e^{\frac{\langle \gamma^p - \gamma_c^p \rangle}{\gamma_c^p}} \tag{33}$$

where $\langle a \rangle = \frac{a+|a|}{2}$ is the Macauley bracket. γ_c^p is a critical value of the generalized plastic strain at failure state. It corresponds to the peak stress in uniaxial compression test. C_1 is a model parameter.

The numerical implementation is based on the standard return mapping algorithm. Due to the material non-linearity, an iterative procedure is needed. Each iteration is composed of elastic prediction and plastic-damage correction. The local integration for calculating instantaneous deformation at kth increment or the cumulative ones at kth cycle is in the following order

(1) At the end of $(k-1)$th loading increment (monotonic phase) or for $(k-1)$th cycle (cyclic phase), $\boldsymbol{\sigma}_{k-1}$, $\boldsymbol{\varepsilon}_{k-1}$, $\boldsymbol{\varepsilon}_{k-1}^p$, $\bar{\omega}_{k-1}$ and ω_{k-1} are known.
(2) Given a new stress increment $\mathrm{d}\boldsymbol{\sigma}$ or a new loading cycle increment $\mathrm{d}n$, then the total stress $\boldsymbol{\sigma}_k = \boldsymbol{\sigma}_{k-1} + \mathrm{d}\boldsymbol{\sigma}$ and total loading cycle $n_k = n_{k-1} + \mathrm{d}n$.
(3) If $\mathrm{d}\boldsymbol{\sigma} \neq \mathbf{0}$ and $\mathrm{d}n = 0$, go to (4); if $\mathrm{d}\boldsymbol{\sigma} = \mathbf{0}$ and $\mathrm{d}n \neq 0$, go to (5).
(4) Check $f(\boldsymbol{\sigma}_k) \leq 0$. If $f(\boldsymbol{\sigma}_k) \leq 0$, $\mathrm{d}\boldsymbol{\varepsilon}_k^p = \mathbf{0}$ and $\mathbb{D}_k^{tan} = \mathbb{D}^0$; else, calculate the plastic multiplier $\mathrm{d}\lambda$ by Eq. (27) and calculate $\mathrm{d}\boldsymbol{\varepsilon}_k^p$ and $\mathbb{D}_k^{tan}$ by Eq. (30). Then go to (6).
(5) Calculate $\bar{\omega}_k$, ω_k and $\dot{\omega}_k$ by Eqs. (33), (32) and (1), respectively. Check $f(\boldsymbol{\sigma}_k) \leq 0$. If $f(\boldsymbol{\sigma}_k) \leq 0$, $\mathrm{d}\boldsymbol{\varepsilon}_k^p = \mathbf{0}$; else calculate $\mathrm{d}\boldsymbol{\varepsilon}_k^p$.
(6) Update $\bar{\omega}_k$ and ω_k, $\boldsymbol{\varepsilon}_k^p$ and $\boldsymbol{\varepsilon}_k = \mathbb{D}_k^0 : \mathrm{d}\boldsymbol{\sigma} + \boldsymbol{\varepsilon}_k^p$ or by (29).

4.2. Application to argillaceous quartz siltstone

Before predicting the cumulative deformation in cyclic loading, the proposed model is firstly applied to study the instantaneous response in conventional triaxial compression tests. The elastic parameters of intact materials E_0 and ν_0, or equivalently k_0 and μ_0, are determined from the linear parts of stress–strain curves. The failure parameters A and C can be easily identified from the peak stress values of triaxial compression tests with different confining stresses. The initial value of hardening function α_p^0 is estimated from the beginning points of plastic deformation. The parameter B can be identified from the evolution of generalized plastic strain. The potential parameter η is determined from the volumetric compressibility–dilatancy transition points.

The mechanical behavior of an argillaceous quartz siltstone is considered. The experimental data reported in Miao et al. (2021b) are used. With the procedure presented above, the values of elastoplastic parameters are given in Table 1. The stress–strain curves in a monotonic uniaxial compression test are presented in Fig. 4. The numerical results provided by the basic elastoplastic model are compared with the experimental data. Although some tiny differences are observed, there is a general satisfactory agreement between the numerical and experimental results for both axial and lateral strains (ϵ_1 and ϵ_3). The proposed model shows the ability for capturing the main features of short-term mechanical property of argillaceous quartz siltstone, both in the elastic and plastic stages. As a result, the parameters listed in Table 1 will be also adopted in the analysis of cyclic loading tests presented below.

Cyclic loading tests were also conducted on argillaceous quartz siltstone (Miao et al., 2021b). The samples were subjected to unloading–reloading cycles with different values of upper limit load. The proposed elastoplastic fatigue-damage model is applied to

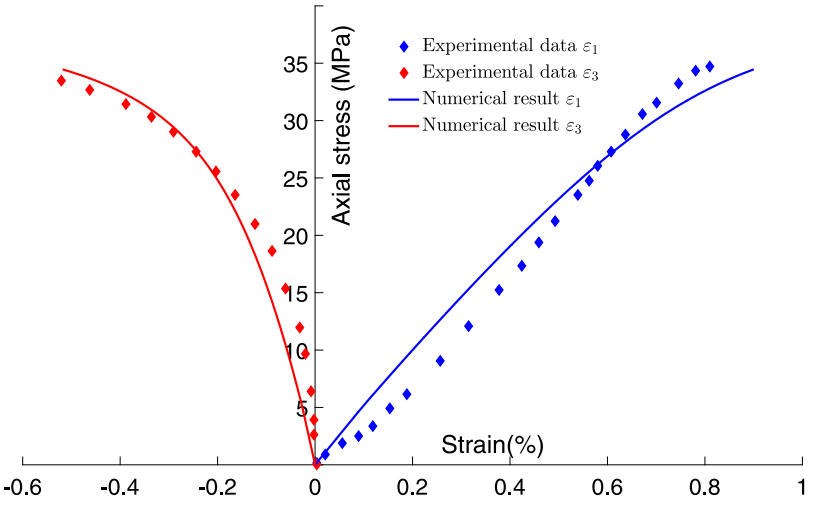

Fig. 4. Comparison between numerical results and experimental data of axial strain ε_1 and lateral strain ε_3 in uniaxial compression test on argillaceous quartz siltstone.

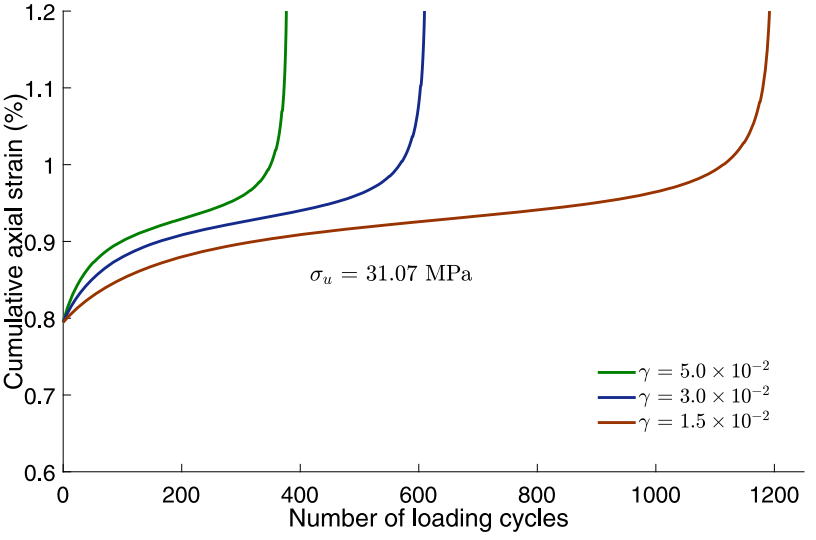

Fig. 5. Parametric study on the influence of the fatigue parameter γ.

the analysis of such cyclic tests, in particular the evolution of accumulated strains with the number of cycles. The total strains are obtained by adding the reversible strains and residual ones reported in the original experimental data (Miao et al., 2021b).

Before carrying out numerical simulation of cyclic tests, we are concerned with the influence of damage evolution parameter γ involved in the final formulation Eq. (29) in Fig. 5. It is seen that the value of γ mainly influences the transient rate from decay stage to accelerated stage. Besides, since only the effects of upper stress σ_u of cyclic loads on the accumulative deformation will be discussed with the experimental data, we will also provide the parametric studies of strength parameter C and the ratio of the upper limit stress and strength σ_u/C by varying their values in Figs. 6 and 7, respectively. We can conclude from Fig. 6 that the fatigue collapse will arrive earlier with the decrease of strength parameter. Similarly, although the strength parameter also gets larger with the increase of applied cyclic stress, keeping a constant ratio σ_u/C, the magnitude of fatigue deformation will increase, as shown in Fig. 7.

The parameters involved in the description of fatigue damage evolution include γ, C_1, α_1 and α_2. They are identified by an optimization procedure by comparing the numerical predictions of cumulative axial strain at peak point of each cycle with the experimental data for the case with an upper limit stress of 31.07 MPa and a lower limit stress of 2.55 MPa. Indeed, for this case, the typical three stages of accumulated strain are obtained as that indicated by the green line in Fig. 1. This facilitates the determination of all involved parameters. The values obtained for the argillaceous siltstone are as $\gamma = 1.5 \times 10^{-2}$, $C_1 = 0.1717$, $\alpha_1 = 0.25$ and $\alpha_2 = 0.652$. The comparison between the fitted numerical results and experimental data are presented in Fig. 8. The obtained values are then used for studying cyclic responses under different limit stresses. A sensitivity study is presented at the end of this section.

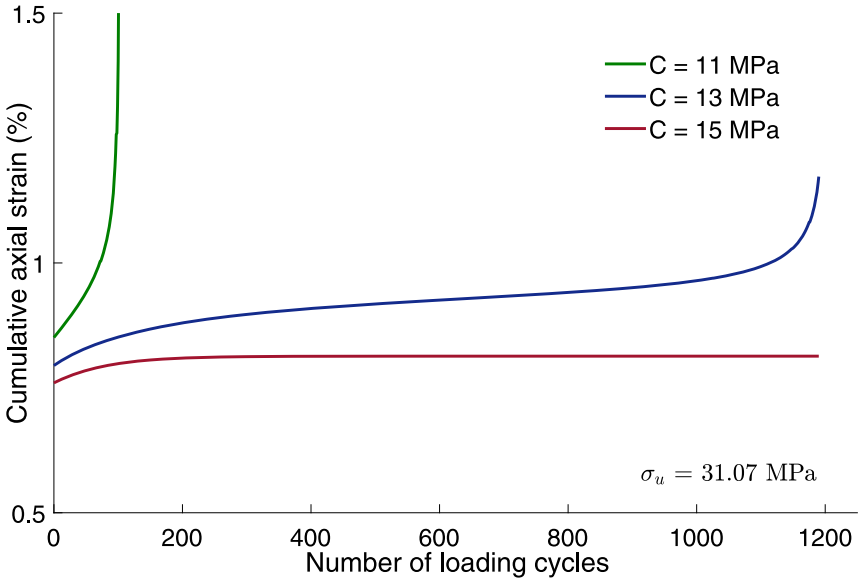

Fig. 6. Parametric study on the influence of strength parameter with constant upper stress $\sigma_u = 31.07$ MPa.

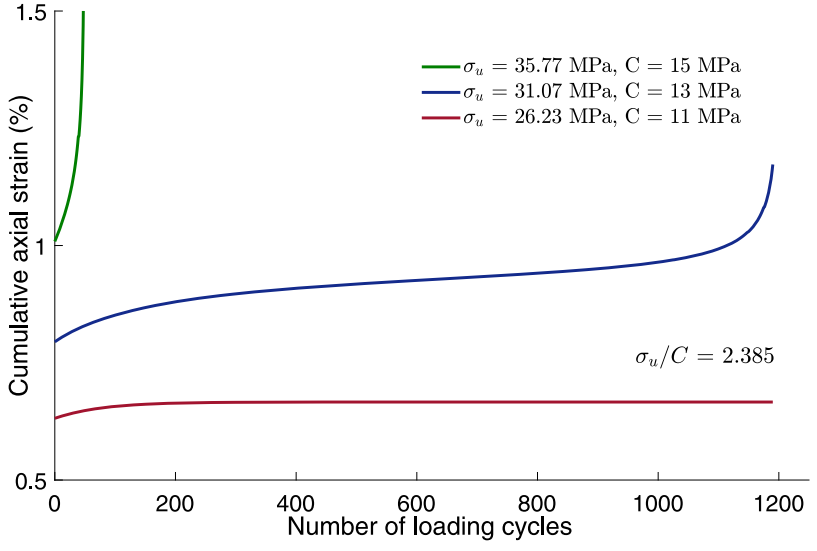

Fig. 7. Parametric study on the influence of strength and upper stress with constant stress ratio $\sigma_u/C = 2.385$.

With the above set of basic mechanical and fatigue damage parameters, the proposed model is used to study the cumulative axial strains in cyclic loading tests, which were performed under the same lower limit stress ($\sigma_l = 2.55$ MPa) but 6 different upper limit stresses ($\sigma_u = 15.28, 20.37, 28.01, 31.07, 31.32$ and 33.1 MPa). The obtained numerical results are compared with the experimental data for axial and lateral deformations in Fig. 9. There is a good agreement for all levels of upper limit stress. Particularly, depending on the applied upper limit stress value, the proposed model is able to reproduce three typical types of fatigue deformation evolution curve. Despite of some differences in the lateral direction close to failure, the evolution trend and fatigue life are well described.

More precisely, for all values of upper limit stress, there is an initial instantaneous deformation at the first cycle, which is described by the short-term elastoplastic model. But the whole evolution of cumulative axial strain and the related fatigue life time are obviously dependent on the upper limit stress. For lower levels, for instance $\sigma_u = 15.28, 20.37$ and 28.01 MPa in Fig. 9, the cumulative axial strain increases rapidly at the decay stage and stabilizes at the steady stage. The value of total cumulative strain is larger when the upper limit stress is higher at the same number of loading cycles. But this is mainly due to the difference on the initial instantaneous strain. The fatigue failure does not occur after 3000 cycles for these three cases. This type of mechanical behavior corresponds to the typical shakedown and high-cycle fatigue state. In order to better understand the coupling between plastic deformation and fatigue damage, the evolution of generalized plastic strain γ_p and that of damage parameter ω are plotted

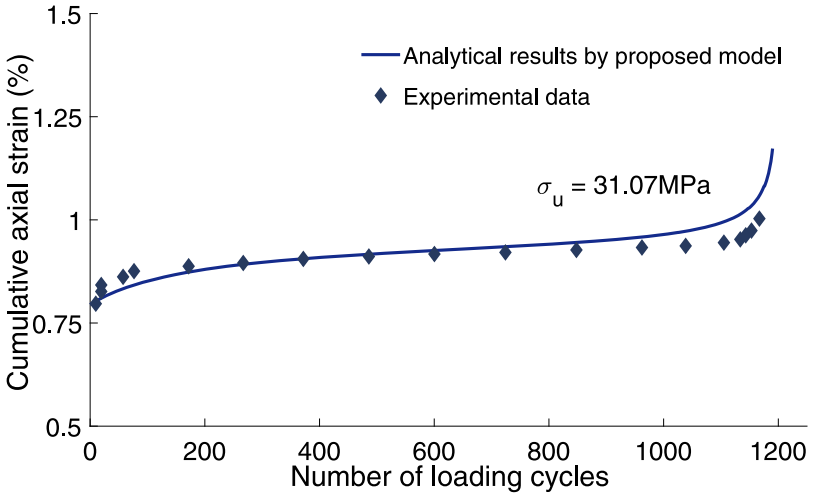

Fig. 8. Comparison of cumulative axial strain of argillaceous siltstone between model's prediction and experimental data for the case used for parameters identification with σ_u = 31.07 MPa.

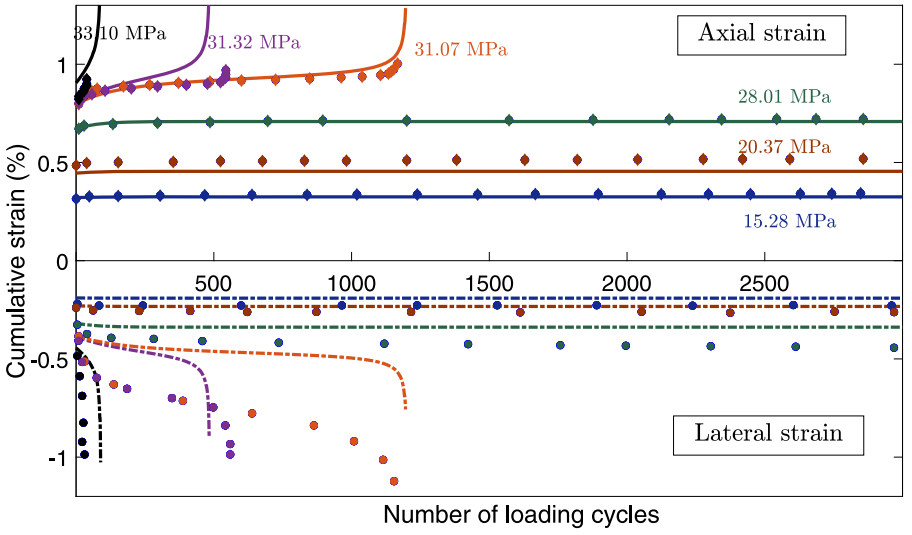

Fig. 9. Evolution of cumulative strain of argillaceous siltstone by cyclic loading tests under different levels of upper limit stress: comparisons between numerical results (Continuous lines: axial strain; dash–dot lines: lateral strain) and experimental data (Solid symbols).

in Figs. 10 and 11, respectively for two stabilized fatigue damage cases σ_u = 15.28 and 28.01 MPa. It is seen that the asymptotic values of damage parameter ω and that of generalized plastic strain γ_p for σ_u = 28.01 MPa (Fig. 11) are higher than those for σ_u = 15.28 MPa (Fig. 10). But in both cases, the fatigue damage indicating the degradation of micro-structure evolves towards a stationary value after the decay stage. There is a strong correlation between the evolution of axial strain (blue solid line) and that of the damage parameter (red dash–dot line).

However it does not mean the material remains always in stable state if the cyclic loading is continually maintained. This is due to the accumulation of irreversible plastic strain energy produced in each stabilized cycle (Dang-Van, 1993; Zhang et al., 2017a), leading to the high-cycle fatigue collapse. Even in a stabilized case with a low upper limit stress, the generalized plastic strain γ_p exhibits a slow growth at the steady stage. Actually, for most rock like materials, the pure elastic shakedown phenomenon is generally not observed in cyclic loading condition, since the material degradation accumulates once the upper limit stress is larger than the initial yield threshold. The applied value of upper limit stress essentially affects the length of fatigue life.

On the other hand, for the cases with a high value of the upper limit stress, an accelerated evolution phase is produced after a more and less large steady stage, as shown in Fig. 9. We consider here in more detail the case with σ_u = 31.07 MPa. The variations of cumulative axial strain, equivalent plastic strain and fatigue damage are presented in Fig. 12. It is found that the steady stage accounts for the major period of fatigue life. However, the accumulated strain during the steady stage represents only a quite small part of the total quantity, indicating a quasi equilibrium state of the micro-structure. Contrarily, the amounts of accumulated strain in

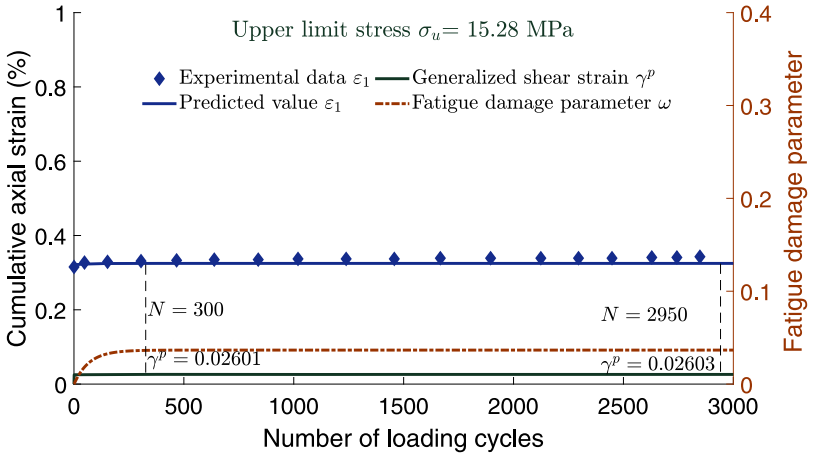

Fig. 10. Variations of cumulative axial strain ε_1, generalized plastic strain γ_p and damage parameter ω for σ_u = 15.28 MPa. (For interpretation of the references to color in this figure legend, the reader is referred to the web version of this article.)

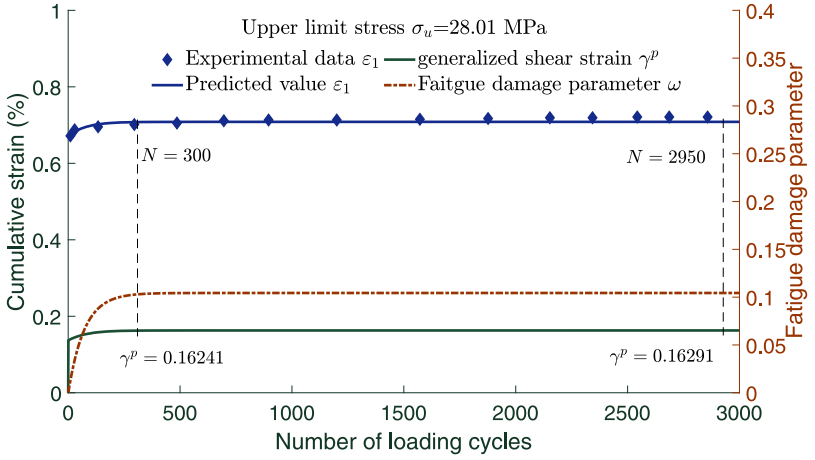

Fig. 11. Variations of cumulative axial strain ε_1, generalized plastic strain γ_p and damage parameter ω for σ_u = 28.01 MPa. (For interpretation of the references to color in this figure legend, the reader is referred to the web version of this article.)

the remaining two stages are considerably larger, but the corresponding periods of loading is shorter. According to most fatigue tests, it is generally observed that the upper limit stress and the amplitude of stress variation have a significant influence on the evolution of irreversible cumulative deformation. By comparing the strain-cycle curves of σ_u = 31.07 MPa with that of σ_u = 31.32 MPa, the steady stage period is significantly reduced leading to a reduction of the fatigue life (1200 → 500). Besides, the accumulated plastic strain in the cyclic loading process also shows an accelerated phase (see green line in Fig. 12), in consistency with the evolution of fatigue damage parameter. When the upper limit stress becomes high enough, the period of steady stage is drastically reduced and even disappears such as the case with σ_u = 33.1 MPa (black line in Fig. 9). The material fails due to an excessive deformation in a very short term, producing the ratcheting in cyclic loading. The underlying mechanism is the rapid growth of material damage.

For a more detailed analysis of accumulated deformation during cyclic loading, the increments of axial strain at each cycle are plotted in Fig. 13, respectively for three different upper limit stresses of 28.01, 31.07 and 31.32 MPa. The numerical solution predicted by the proposed model and experimental results reported in Miao et al. (2021b) are compared. In general, a good agreement can be observed. For the lower stress level (σ_u = 28.01 MPa) with no accelerated stage, the increment of axial strain exhibits a rapid decent after the first cycle and varies around zero value until 3000 cycles. For higher stress levels (σ_u = 31.07 and 31.32 MPa), the curves of axial strain increment shows a U-shape. The axial strain increment also descends after the first cycle, but increases rapidly in the accelerated stage.

In Fig. 14, one displays the evolution of Young's modulus during cyclic loading with the increase of fatigue damage for two different upper limit stresses. The curves of Young's modulus exhibit a general inverse shape with those of damage parameter, obeying the linear relation Eq. (14). It is clear that the fatigue-induced degradation of micro-structure leads to a progressive decrease of Young's modulus. Further, the degradation rate of Young's modulus is higher for σ_u = 31.07 MPa (green line) than that for σ_u = 28.01 MPa (red line), in particular at the decent and accelerated stages. The elastic modulus for σ_u = 28.01 MPa becomes nearly

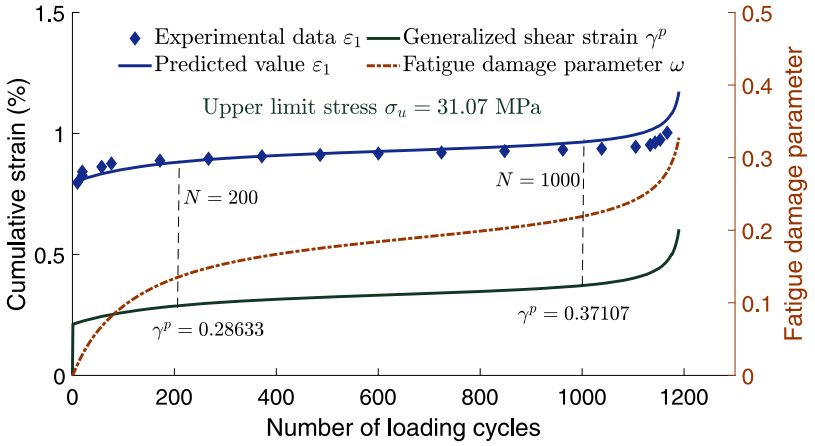

Fig. 12. Variations of accumulated axial strain ε_1, generalized plastic strain γ_p and damage parameter ω for σ_u = 31.07 MPa. (For interpretation of the references to color in this figure legend, the reader is referred to the web version of this article.)

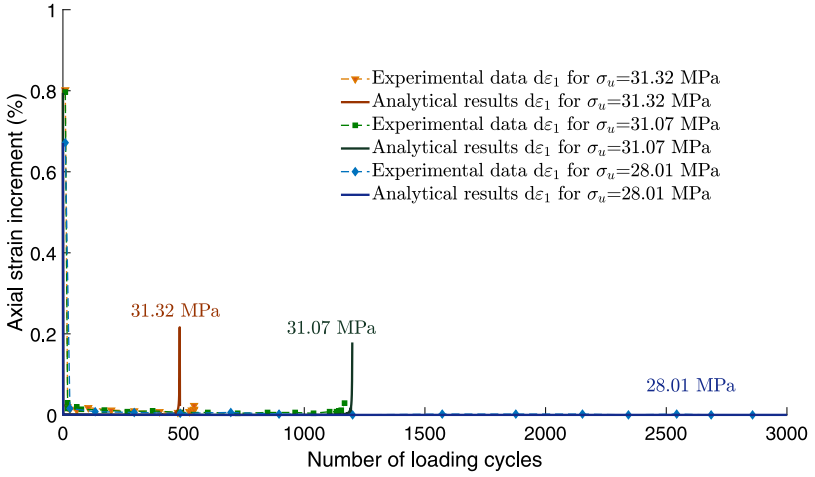

Fig. 13. Increment of axial strain ε_1 at each cycle for three different upper limit stresses of 28.01, 31.07 and 31.32 MPa.

stationary after the decay stage, while that for σ_u = 31.07 MPa decreases approximately linearly in the steady stage and falls off a cliff around the fatigue failure. Considering the linear relation between the damage parameter and the elastic constant in Eq. (14), the different shapes of Young's modulus evolution curve are consistent with those of the damage parameter (see Figs. 11 and 12), reflecting the micro-structure degradation of material.

In Fig. 15, we show the evolution of fatigue damage parameter ω and its asymptotic value $\bar{\omega}$ for three different upper limit stresses. It should be pointed out that the evolution curves of ω (dash–dot lines) are the same as those plotted in Figs. 11 and 12. The corresponding variations of $\bar{\omega}$ are illustrated by the solid lines. It is seen that the stationary condition of fatigue damage, that is $\omega \to \bar{\omega}$, is progressively approached during the cyclic loading history. The evolution of ω starts from zero value at the first cycle, while the initial value of $\bar{\omega}$ depends on the prescribed upper limit stress. More precisely, for a lower limit stress of σ_u = 28.01 MPa, the fatigue damage parameter reaches rapidly the value of $\bar{\omega}$ and holds at a stationary value. There is no fatigue failure of material at least within 2500 cycles. On the contrary, under a higher limit stress of σ_u = 31.07 MPa, although the value of ω is quite close to that of $\bar{\omega}$, the fatigue failure still occurs due to the rapid increase of $\bar{\omega}$, reflecting the unstable degradation of micro-structure. At last, for σ_u = 33.10 MPa, the stationary value $\bar{\omega}$ is never approached by ω, but the ratcheting type failure is obtained in a very short term with a very short steady stage.

In order to better identify the effect of upper limit stress on th failure mechanisms of argillaceous quartz siltstone subjected to cyclic loading, the evolution of cumulative axial strain is investigated again with respect to some selected values of upper limit stress. The obtained results are presented in Fig. 16. Inspired by the definition of high cycle fatigue (HCF≥1e4 cycles) and low cycle fatigue (1e3≥LCF≥1e4 cycles), the strain-cycle curve in Fig. 16 is divided into 3 regions by the value of upper limit stress. For σ_u < 30.9965 MPa, the region is defined as the high cycle fatigue or shakedown where the cumulative strain maintains at a stationary value, and the material will not fail within 10 000 cycles. In terms of shakedown theory, the total energy is not bounded

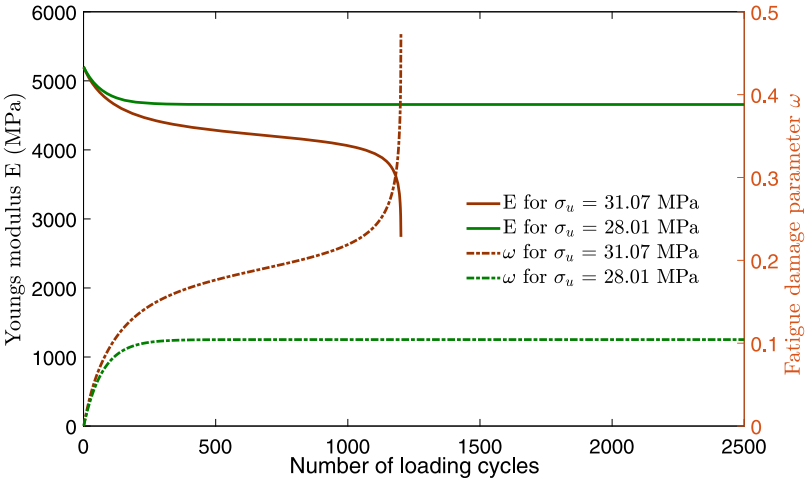

Fig. 14. Progressive degradation of Young's modulus during cyclic loading with the increase of fatigue damage for two different upper limit stresses. (For interpretation of the references to color in this figure legend, the reader is referred to the web version of this article.)

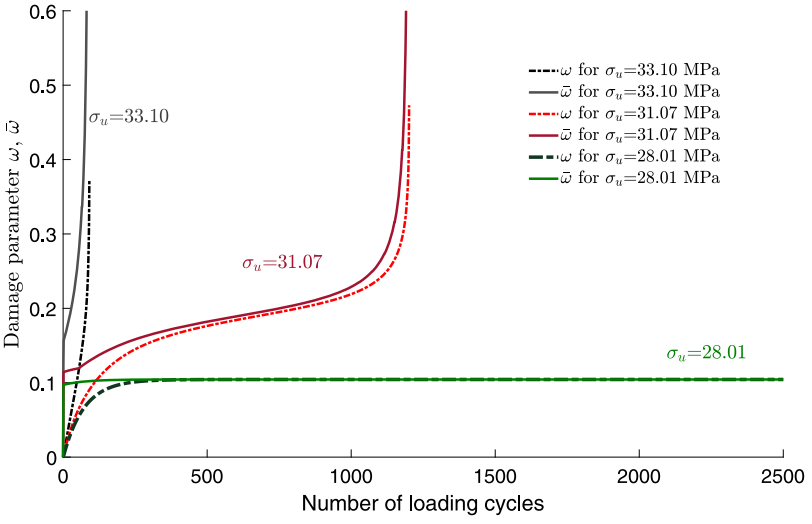

Fig. 15. Evolution of fatigue damage parameter ω and its stationary value $\bar{\omega}$ under different upper limit stresses.

and accumulated in each cycle, although the deformation is not obviously increased. However, as mentioned above, the shakedown behavior is rarely observed once the applied load is beyond the elastic limit. The failure mode in the region 30.9965 MPa $< \sigma_u <$ 31.1 MPa is defined as the low cycle fatigue one, where the material can bear more than 1000 cycles. In this region, the cumulative strain increases slowly in most loading process, and a sudden acceleration is observed near the fatigue collapse of the material. Finally, the ratcheting failure, where the cumulative strain increases consistently, occurs for $\sigma_u >$ 31.1 MPa. In this region, the fatigue life of material is inferior to 1000 cycles. It is noticed that the failure mechanism of the siltstone is very sensitive to the upper limit stress of the cyclic loading. In particular, the transient interval from the low cycle fatigue to ratcheting is only about 0.1 MPa (30.9965 to 31.1). This is also the reason that the full 3-stage axial strain curve in Fig. 8 is used for the identification of model's parameters.

4.3. Application to salt rock

Aiming at verifying the prediction ability of the proposed elastoplastic fatigue-damage model for different types of rocks, the mechanical behavior of salt rock under cyclic loading is investigated in this subsection. The experimental data are taken from the previous work reported in Fuenkajorn and Phueakphum (2010). By using the same strategy for the determination of model parameters as described before, the typical values of elastic–plastic and fatigue-damage evolution parameters of salt rock are listed in Table 2.

The stress–strain curve in monotonic uniaxial compression test is presented in Fig. 17. It is seen that the proposed elastoplastic model is able to capture the basic mechanical response of salt rock in uniaxial compression test for the whole loading process. The

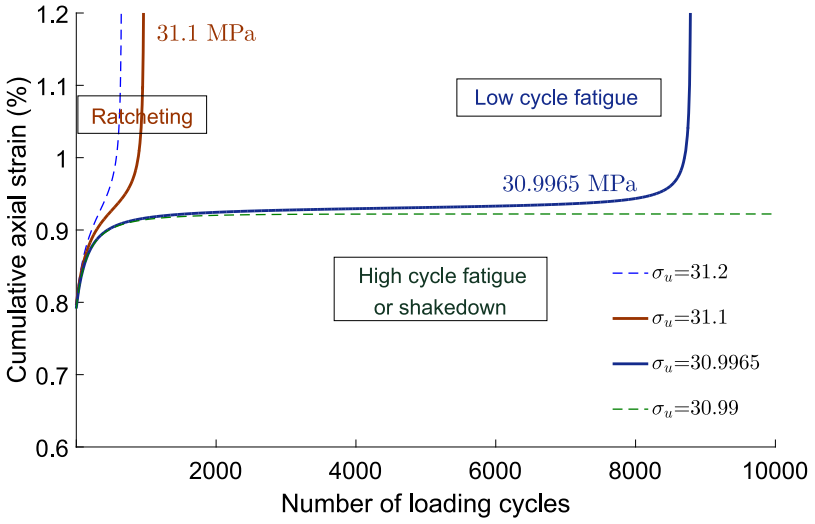

Fig. 16. Different regions of fatigue failure mechanism for argillaceous quartz siltstone.

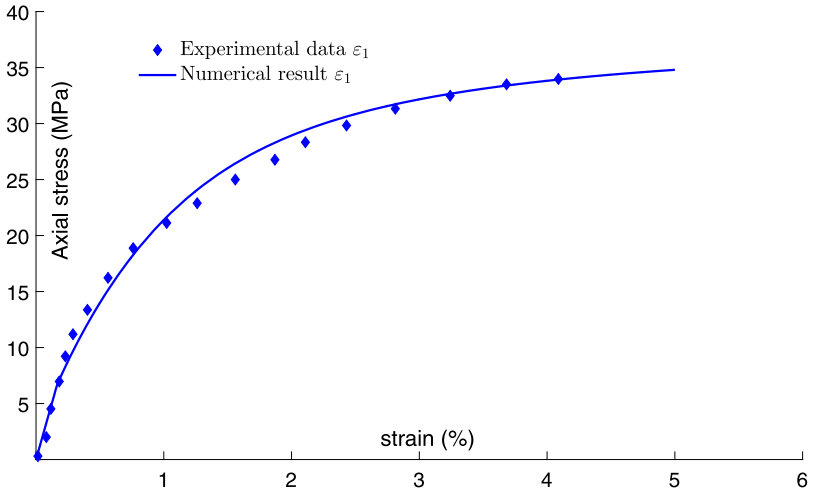

Fig. 17. Comparison of numerical and experimental results of salt rock in uniaxial compression test.

Table 2
Typical parameters adopted for Maha Sarakham salt rock.

E (MPa)	ν	A_0(MPa)	C_0	α_p^0	B	η	γ	α_1	α_2	C_1
4048	0.2	53.15	15.24	0.05	0.00885	−0.0012	8.8e−5	2.25	1.31	0.5

deformation at failure state of salt rock is significantly larger than that of argillaceous siltstone, while the peak stresses of the two rocks are quite similar each to other. The salt rock has a smaller elastic stiffness and exhibits a more important plastic deformation. It is worth noticing that the lateral strain is not presented in this figure due to the lack of experimental data.

The evolution curves of cumulative axial strain are presented in Fig. 18 for four different values of upper limit stress (σ_u = 21.4, 24.9, 28.1 and 30.0 MPa). Again, it is clearly seen that the numerical predictions of cumulative axial strain by the proposed model are in a very good accordance with the experimental results. The fatigue lifetime behavior of salt rock is well described. As a result, the novel elastoplastic fatigue-damage model is able to describe the progressive deformation and fatigue damage of different types of rocks subjected to cyclic loading. As for the argillaceous siltstone, the fatigue life is significantly reduced with the increase of upper limit stress. However, unlike the argillaceous siltstone, there is no evident steady stage observed in Fig. 18, and the failure due to an excessive deformation occurs for all values of upper limit stress. The reasons for this phenomenon are multiple, but mainly related to the high stress level used in the experiment and large inelastic strain accumulated in each cycle (as shown in Fig. 17). The fatigue damage rate of salt rock is more rapid than that of siltstone, leading to a short fatigue lifetime of the material.

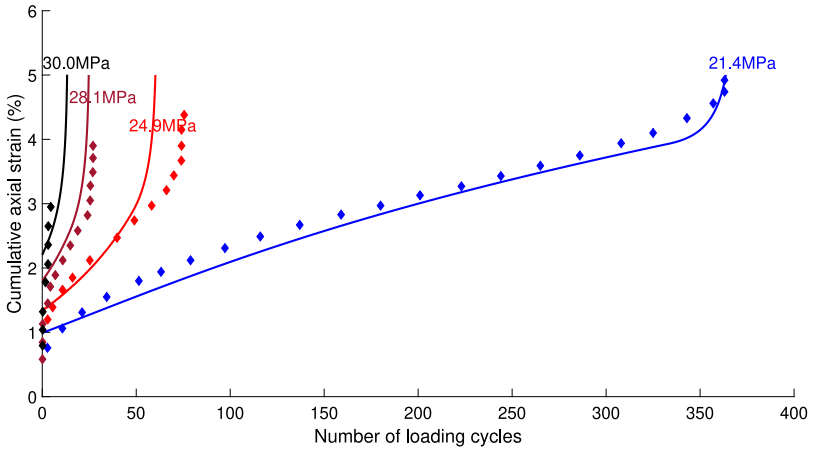

Fig. 18. Cumulative axial strain of salt rock in cyclic loading tests with different values of upper limit stress; comparisons between numerical results (continuous lines) and experimental data (diamond symbols).

Table 3
Identified values of elastic–plastic parameters for multilevel cyclic test.

E (MPa)	ν	A_0	C (MPa)	α_p^0	B	η
3400	0.2	53	13	0.0017	0.0021	−0.0012

The proposed elastic–plastic damage model (29) is constructed from the perspective of directly predicting the total strain in cyclic tests by identifying the upper limit stress and loading cycles. The total deformation in loading process and cyclic process can be both calculated by the unified formulation. In order to confirm the accuracy, we have performed another application to multilevel cyclic loading tests on salt samples (Zhao et al., 2022) collected from a Pakistan salt mine. The maximum cyclic stress at the first stage is 10 MPa and increased by 2 MPa for the next stage, and each loading stage contains 20 cycles. The minimum cyclic stress keeps 5 MPa in all cyclic stages. The values of elastoplastic parameters are given in Table 3. The corresponding fatigue damage values are as $\gamma = 3.7 \times 10^{-4}$, $C_1 = 0.2137$, $\alpha_1 = 0.25$ and $\alpha_2 = 0.652$.

The comparison between the numerical predictions and experimental strain–stress cyclic curves are illustrated in Fig. 19. Noting that the pore compaction stage in the first cycle is neglected. The mechanical responses in loading period are noted as blue lines and the cumulative strains in cyclic period are in red. A good agreement can be observed. The total deformation throughout the process of multilevel cyclic tests can be easily predicted by the proposed model.

5. Conclusion

A novel elastoplastic fatigue-damage model is developed to describe the mechanical behavior of rock materials under monotonic and cyclic loading conditions. The induced fatigue damage is physically related to material micro-structural degradation and it is described by a convolutional law. Moreover, the evolution of fatigue damage is explicitly coupled with the plastic deformation. The upper limit stress has an essential influence on the plastic deformation, and is the main factor affecting the fatigue life of materials. The proposed model is formulated for both stress and strain-prescribed loading paths in view of engineering application. A convenient strategy is proposed for the determination of parameters involved in the new model.

The proposed model is applied to two representative rocks, argillaceous quartz siltstone and salt rock, which were investigated in monotonic and cyclic laboratory tests. A general good agreement is obtained for both rocks either for deformation and fatigue lifetime responses, showing a broad applicability of the model for different types of rocks. The evolution of fatigue damage, accumulated total and plastic strains, and fatigue lifetime under different values of upper limit stress is discussed in detail. Different fatigue failure mechanisms are analyzed. It is found that the transient interval from the low cycle fatigue to ratcheting is very sensitive to the upper limit stress. As for future work, the coupling between time-dependent deformation of rocks and fatigue damage evolution will be taken into account.

CRediT authorship contribution statement

J. Zhang: Completed the theoretical formulation, Participated in numerical modeling and the interpretation of results, Writing of the manuscript. **W.Y. Liu:** Participated in the numerical calculations, Analysis of results. **Q.Z. Zhu:** Theoretical development, Setting of numerical algorithms. **J.F. Shao:** Designed the theoretical framework, Participated in the analysis of results, Writing and revision of the manuscript.

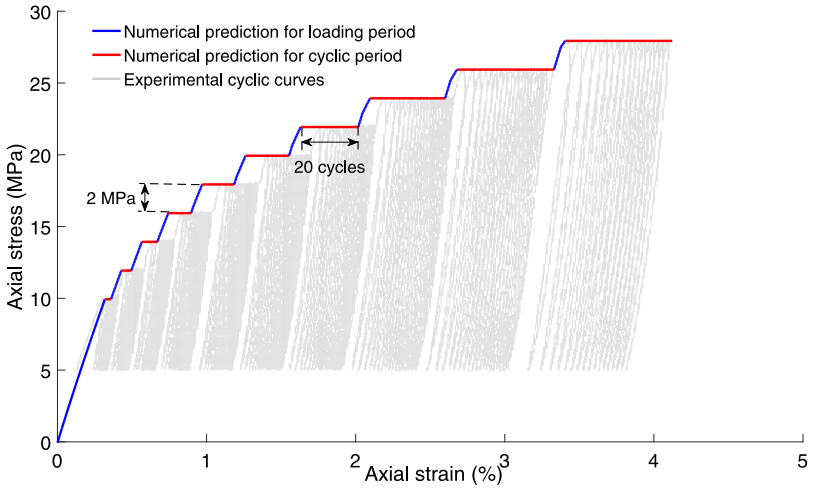

Fig. 19. Prediction of cumulative strain in multilevel cyclic loading test with constant stress intervals. (For interpretation of the references to color in this figure legend, the reader is referred to the web version of this article.)

Declaration of competing interest

The authors declare that they have no known competing financial interests or personal relationships that could have appeared to influence the work reported in this paper.

Data availability

Data will be made available on request.

Acknowledgments

The authors would like to thank the National Natural Science Foundation of China (Grant No. 11902111) for the support.

Appendix A. Derivation of the mathematical formulation of fatigue damage factor (3)

In the present study, the fatigue damage parameter ω is a function of the cumulative plastic strain ε_{ij}^{p} at the peak of each cycle and number of loading cycles n:

$$\omega = \omega\left(\varepsilon_{ij}^{p},\, n\right) \tag{34}$$

and the rate of damage evolution is described by a linear relation:

$$\dot{\omega} = \gamma\left(\bar{\omega} - \omega\right) \tag{35}$$

The function ω can be formally defined by employing the Laplace transform. Noting that

$$\mathcal{L}\left(\dot{\omega}\right) = s\mathcal{L}\left(\omega\right) - \mathcal{L}\left(\omega\right) \tag{36}$$

taking $\bar{\omega} > \omega$ and initial condition $\omega(0) = 0$, we have

$$\gamma\left(\mathcal{L}\left(\bar{\omega}\right) - \mathcal{L}\left(\omega\right)\right) = s\mathcal{L}\left(\omega\right) \tag{37}$$

Thus

$$\mathcal{L}\left(\omega\right) = \frac{\gamma}{\gamma + s}\mathcal{L}\left(\bar{\omega}\right) \tag{38}$$

Furthermore, noting that

$$\frac{\gamma}{\gamma + s} = \mathcal{L}\left(\gamma e^{-\gamma n}\right) \tag{39}$$

Eq. (38) can be expressed as

$$\mathcal{L}\left(\omega\right) = \mathcal{L}\left(\gamma e^{-\gamma n}\right)\,\mathcal{L}\left(\bar{\omega}\right) \tag{40}$$

Employing now the convolution theorem, one obtains

$$\omega = \int_0^N \bar{\omega}(n)\gamma e^{-\gamma(N-n)}\mathrm{d}n \tag{41}$$

As a result, upon integrating by parts

$$\omega = \bar{\omega} - \int_0^N \frac{\partial \bar{\omega}}{\partial n} e^{-\gamma(N-n)}\mathrm{d}n \tag{42}$$

Thus, the evolution parameter ω depends on the history of the time derivative of $\bar{\omega}$, whereas the exponential term represents the memory function.

Appendix B. Non-linear explicit integral algorithm for fatigue cumulative deformation

With the loading history of N cycles, the fatigue damage parameter of material ω_N can be computed by employing the convolution theorem

$$\omega_N = \int_0^N \bar{\omega}(n)\gamma e^{-\gamma(N-n)}\mathrm{d}n \tag{43}$$

which can be rewritten as

$$\omega_N e^{\gamma N} = \gamma \int_0^N \bar{\omega}(n) e^{\gamma n}\mathrm{d}n \tag{44}$$

Similarly, for the loading interval until the previous increment $[0, N-\mathrm{d}n]$, the corresponding fatigue damage parameter reads

$$\omega_{N-\mathrm{d}n} e^{\gamma(N-\mathrm{d}n)} = \gamma \int_0^{N-\mathrm{d}n} \bar{\omega}(n) e^{\gamma n}\mathrm{d}n \tag{45}$$

Subtract (45) from (44), one has

$$\omega_N e^{\gamma N} - \omega_{N-\mathrm{d}n} e^{\gamma(N-\mathrm{d}n)} = \gamma \int_0^N \bar{\omega}(n) e^{\gamma n}\mathrm{d}n - \gamma \int_0^{N-\mathrm{d}n} \bar{\omega}(n) e^{\gamma n}\mathrm{d}n \tag{46}$$

The terms in the left part of Eq. (46) can be reformed as

$$\omega_N e^{\gamma N} - \omega_{N-\mathrm{d}n} e^{\gamma(N-\mathrm{d}n)} = e^{\gamma N}\left(\omega_N - \omega_{N-\mathrm{d}n} e^{\gamma}\right) \tag{47}$$

And the right part is rewritten as

$$\begin{aligned} &\gamma \int_0^N \bar{\omega}(n) e^{\gamma n}\mathrm{d}n - \gamma \int_0^{N-\mathrm{d}n} \bar{\omega}(n) e^{\gamma n}\mathrm{d}n \\ &= \gamma \sum_{i=1}^{N} \left(\frac{\bar{\omega}_i + \bar{\omega}_{i-1}}{2}\right) e^{\gamma\left(n_i - \frac{1}{2}\mathrm{d}n\right)}\mathrm{d}n - \gamma \sum_{i=1}^{N-1} \left(\frac{\bar{\omega}_i + \bar{\omega}_{i-1}}{2}\right) e^{\gamma\left(n_i - \frac{1}{2}\mathrm{d}n\right)}\mathrm{d}n \\ &= \gamma \left(\frac{\bar{\omega}_i + \bar{\omega}_{i-1}}{2}\right) e^{\gamma\left(n_i - \frac{1}{2}\mathrm{d}n\right)}\mathrm{d}n \end{aligned} \tag{48}$$

Taking (47) and (48) into (46) and considering $\mathrm{d}n = 1$, the final expression of the fatigue damage parameter at Nth loading cycle is in the following form

$$\omega_N = \omega_{N-1} e^{-\gamma \mathrm{d}n} + \gamma \left(\frac{\bar{\omega}_i + \bar{\omega}_{i-1}}{2}\right) e^{\gamma\left(n_i - \frac{1}{2}\mathrm{d}n\right)}\mathrm{d}n \tag{49}$$

The above formulation is applied to compute the damage factor in the cyclic loading process by the proposed constitutive model. It can be seen that from the non-linear explicit algorithm (49), only the variables ω_{n-1}, $\bar{\omega}_{n-1}$ and $\bar{\omega}_n$ need to be stored in the computation procedure. Consequently, the computational efficiency is greatly improved by comparing to traditional integration algorithms. It should be pointed out that the above algorithm is firstly provided in the creep study (Zhu et al., 2016a) by considering the integral variable of time.

References

Abu-Lebdeh, T.M., Voyiadjis, G.Z., 1993. Plasticity-damage model for concrete under cyclic multiaxial loading. J. Eng. Mech. 119 (7), 1465–1484.

Baktheer, A., Aguilar, M., Chudoba, R., 2021. Microplane fatigue model MS1 for plain concrete under compression with damage evolution driven by cumulative inelastic shear strain. Int. J. Plast. 143, 102950.

Cao, Y., Wang, W., Shen, W., Cui, X., Shao, J., 2022. A new hybrid phase-field model for modeling mixed-mode cracking process in anisotropic plastic rock-like materials. Int. J. Plast. 157, 103395.

Carol, I., Bazant, Z.P., 1997. Damage and plasticity in microplane theory. Int. J. Solids Struct. 34 (29), 3807–3835.

Cerfontaine, B., Charlier, R., Collin, F., Taiebat, M., 2017. Validation of a new elastoplastic constitutive model dedicated to the cyclic behaviour of brittle rock materials. Rock Mech. Rock Eng. 50 (10), 2677–2694.

Chen, W., Li, S., Li, L., Shao, M., 2020. Strengthening effects of cyclic load on rock and concrete based on experimental study. Int. J. Rock Mech. Min. Sci. 135, 104479.

Chiarelli, A., 2000. Experimental Investigation and Constitutive Modeling of Coupled Elastoplastic Damage in Hard Claystones (Ph.D. thesis). University of Lille.
Dang-Van, K., 1993. Macro-micro approach in high-cycle multiaxial fatigue. In: Advances in Multiaxial Fatigue. ASTM International.
Dragon, A., Mroz, Z., 1979. A continuum model for plastic-brittle behaviour of rock and concrete. Internat. J. Engrg. Sci. 17 (2), 121–137.
Fan, J., Chen, J., Jiang, D., Ren, S., Wu, J., 2016. Fatigue properties of rock salt subjected to interval cyclic pressure. Int. J. Fatigue 90, 109–115.
François, B., Dascalu, C., 2010. A two-scale time-dependent damage model based on non-planar growth of micro-cracks. J. Mech. Phys. Solids 58 (11), 1928–1946.
Frantziskonis, G., Desai, C., 1987. Elastoplastic model with damage for strain softening geomaterials. Acta Mech. 68 (3), 151–170.
Fuenkajorn, K., Phueakphum, D., 2010. Effects of cyclic loading on mechanical properties of Maha Sarakham salt. Eng. Geol. 112 (1–4), 43–52.
Guo, Y., Zhao, K., Sun, G., Yang, C., Hong-Ling, M., Zhang, G., 2011. Experimental study of fatigue deformation and damage characteristics of salt rock under cyclic loading. Rock Soil Mech. 32 (5), 1353–1359.
Han, S., Yang, X., Shi, D., Miao, G., Huang, J., Li, R., 2020. Microstructure-sensitive modeling of competing failure mode between surface and internal nucleation in high cycle fatigue. Int. J. Plast. 126, 102622.
He, M., Li, N., Zhu, C., Chen, Y., Wu, H., 2019. Experimental investigation and damage modeling of salt rock subjected to fatigue loading. Int. J. Rock Mech. Min. Sci. 114, 17–23.
Huang, Y., Guéry, A.A.-C., Shao, J.-F., 2015. Incremental variational approach for time dependent deformation in clayey rock. Int. J. Plast. 64, 88–103.
Jason, L., Huerta, A., Pijaudier-Cabot, G., Ghavamian, S., 2006. An elastic plastic damage formulation for concrete: Application to elementary tests and comparison with an isotropic damage model. Comput. Methods Appl. Mech. Engrg. 195 (52), 7077–7092.
Jian-po, L., Yuan-hui, L., Shi-da, X., Shuai, X., Chang-yu, J., 2015. Cracking mechanisms in granite rocks subjected to uniaxial compression by moment tensor analysis of acoustic emission. Theor. Appl. Fract. Mech. 75, 151–159.
Kobayashi, H., Kusumoto, T., Nakazawa, H., 1992. The cyclic J-R curve and upper-limit characteristic of fatigue-crack growth in 2-1/2 Cr-Mo steel. Int. J. Press. Vessels Pip. 52 (52), 337–356.
Lee, J., Fenves, G.L., 1998. Plastic-damage model for cyclic loading of concrete structures. J. Eng. Mech. 124 (8), 892–900.
Liu, Y., Dai, F., 2018. A damage constitutive model for intermittent jointed rocks under cyclic uniaxial compression. Int. J. Rock Mech. Min. Sci. 103, 289–301.
Liu, Y., Dai, F., Zhao, T., Xu, N.-w., 2017. Numerical investigation of the dynamic properties of intermittent jointed rock models subjected to cyclic uniaxial compression. Rock Mech. Rock Eng. 50 (1), 89–112.
Liu, F., Fu, Q., Chen, C., Liang, N., 2011. An elasto-plastic damage constitutive theory and its prediction of evolution of subsequent yield surfaces and elastic constants. Int. J. Plast. 27 (9), 1355–1383.
Liu, E., He, S., 2012. Effects of cyclic dynamic loading on the mechanical properties of intact rock samples under confining pressure conditions. Eng. Geol. 125, 81–91.
Liu, X., Ning, J., Tan, Y., Gu, Q., 2016. Damage constitutive model based on energy dissipation for intact rock subjected to cyclic loading. Int. J. Rock Mech. Min. Sci. 85, 27–32.
Luccioni, B.M., Rougier, V.C., 2005. A plastic damage approach for confined concrete. Comput. Struct. 83 (27), 2238–2256.
Mazzucco, G., Pomaro, B., Xotta, G., Maiorana, C.E., Salomoni, V.A., 2020a. Tomography reconstruction of concrete materials for mesoscale modelling. Eng. Comput..
Mazzucco, G., Pomaro, B., Xotta, G., Salomoni, V.A., Majorana, C.E., 2020b. An efficient geometric reconstruction of mesoscale concrete structures accounting for confinement scenarios. Int. J. Multiscale Comput. Eng. 18 (1).
Meng, Q., Zhang, M., Han, L., Pu, H., Chen, Y., 2018. Acoustic emission characteristics of red sandstone specimens under uniaxial cyclic loading and unloading compression. Rock Mech. Rock Eng. 51 (4), 969–988.
Miao, S., Liu, Z., Zhao, X., Huang, Z., 2021a. Energy dissipation and damage characteristics of Beishan granite under cyclic loading and unloading. Chin. J. Rock Mech. Eng. 40, 928–938.
Miao, S., Wang, H., Huang, Z., Liang, M., 2021b. Experimental study on the mechanical properties of argillaceous quartz siltstone under different upper limit cyclic loadings. Eng. Mech. 38 (7), 75–85.
Moreo, P., Garcia-Aznar, J., Doblare, M., 2007. A coupled viscoplastic rate-dependent damage model for the simulation of fatigue failure of cement–bone interfaces. Int. J. Plast. 23 (12), 2058–2084.
Naderloo, M., Moosavi, M., Ahmadi, M., 2019. Using acoustic emission technique to monitor damage progress around joints in brittle materials. Theor. Appl. Fract. Mech. 104, 102368.
Park, T., Ahmed, B., Voyiadjis, G.Z., 2022. A review of continuum damage and plasticity in concrete: Part I–Theoretical framework. Int. J. Damage Mech. 31 (6), 901–954.
Pietruszczak, S., Jiang, J., Mirza, F., 1988. An elastoplastic constitutive model for concrete. Int. J. Solids Struct. 24 (7), 705–722.
Pietruszczak, S., Lydzba, D., Shao, J.-F., 2004. Description of creep in inherently anisotropic frictional materials. J. Eng. Mech. 130 (6), 681–690.
Qu, P.-F., Zhu, Q.-Z., Sun, Y.-F., 2019. Elastoplastic modelling of mechanical behavior of rocks with fractional-order plastic flow. Int. J. Mech. Sci. 163, 105102.
Ren, C., Yu, J., Liu, X., Zhang, Z., Cai, Y., 2022. Cyclic constitutive equations of rock with coupled damage induced by compaction and cracking. Int. J. Mining Sci. Technol..
Sandoval, C., Malcher, L., Canut, F., Araújo, L., Doca, T., Araújo, J., 2020. Micromechanical Gurson-based continuum damage under the context of fretting fatigue: influence of the plastic strain field. Int. J. Plast. 125, 235–264.
Shao, J.-F., Jia, Y., Kondo, D., Chiarelli, A.-S., 2006. A coupled elastoplastic damage model for semi-brittle materials and extension to unsaturated conditions. Mech. Mater. 38 (3), 218–232.
Shao, J.F., Zhu, Q.Z., Su, K., 2003. Modeling of creep in rock materials in terms of material degradation. Comput. Geotech. 30 (7), 549–555.
Song, Z., Konietzky, H., Frühwirt, T., 2018. Hysteresis energy-based failure indicators for concrete and brittle rocks under the condition of fatigue loading. Int. J. Fatigue 114, 298–310.
Spiliopoulos, K.V., Panagiotou, K.D., 2017. An enhanced numerical procedure for the shakedown analysis in multidimensional loading domains. Comput. Struct. 193 (dec.), 155–171.
Surmiri, A., Nayebi, A., Rokhgireh, H., 2018. Shakedown-ratcheting analysis of Bree's problem by anisotropic continuum damage mechanics coupled with nonlinear kinematic hardening model. Int. J. Mech. Sci. 137, 295–303.
Toro, S., Sánchez, P.J., Blanco, P.J., De Souza Neto, E.A., Huespe, A.E., Feijóo, R.A., 2016. Multiscale formulation for material failure accounting for cohesive cracks at the macro and micro scales. Int. J. Plast. 76, 75–110.
Voyiadjis, G.Z., Taqieddin, Z.N., Kattan, P.I., 2008. Anisotropic damage–plasticity model for concrete. Int. J. Plast. 24 (10), 1946–1965.
Voyiadjis, G.Z., Zhou, Y., Kattan, P.I., 2022. A new anisotropic elasto-plastic-damage model for quasi-brittle materials using strain energy equivalence. Mech. Mater. 165, 104163.
Wang, Z., Li, S., Qiao, L., Zhao, J., 2013. Fatigue behavior of granite subjected to cyclic loading under triaxial compression condition. Rock Mech. Rock Eng. 46 (6), 1603–1615.
Wang, Y., Ma, L., Fan, P., Chen, Y., 2016. A fatigue damage model for rock salt considering the effects of loading frequency and amplitude. Int. J. Mining Sci. Technol. 26 (5), 955–958.
Wang, J., Zhang, Q., Song, Z., Feng, S., Zhang, Y., 2022. Nonlinear creep model of salt rock used for displacement prediction of salt cavern gas storage. J. Energy Storage 48, 103951.
Wang, J., Zhang, Q., Song, Z., Zhang, Y., 2021. Experimental study on creep properties of salt rock under long-period cyclic loading. Int. J. Fatigue 143, 106009.

Wu, J.Y., Li, J., Faria, R., 2006. An energy release rate-based plastic-damage model for concrete. Int. J. Solids Struct. 43 (3–4), 583–612.
Xiao, J.-Q., Ding, D.-X., Xu, G., Jiang, F.-L., 2009. Inverted S-shaped model for nonlinear fatigue damage of rock. Int. J. Rock Mech. Min. Sci. 46 (3), 643–648.
Xiao, J.-Q., Feng, X.-T., Ding, D.-X., Jiang, F.-L., 2011. Investigation and modeling on fatigue damage evolution of rock as a function of logarithmic cycle. Int. J. Numer. Anal. Methods Geomech. 35 (10), 1127–1140.
Xu, J., Li, S.-c., Tao, Y.-q., Tang, X.-j., Wu, X., 2009. Acoustic emission characteristic during rock fatigue damage and failure. Procedia Earth Planet. Sci. 1 (1), 556–559.
Xu, B., Liu, X., Zhou, X., Huang, J., Wang, L., Lin, G., Wang, J., Zhang, J., 2022. Investigations on the macro-meso cumulative damage mechanism of the discontinuities in soft-hard interbedded rock mass under pre-peak cyclic shear loading. Int. J. Rock Mech. Min. Sci. 158, 105184.
Xu, Q., Lu, Z., 2013. An elastic–plastic cohesive zone model for metal–ceramic interfaces at finite deformations. Int. J. Plast. 41, 147–164.
Xue, D., Gao, L., Lu, L., Zhou, J., Zhou, H., Wu, Z., Yi, H., Liu, J., 2020. An acoustic emission-based cluster damage model for simulating triaxial compression behaviors of granite. Rock Mech. Rock Eng. 53 (9), 4201–4220.
Yang, D., Hu, J., Ma, S., Zeng, P., 2022. Analysis of dynamic fracture of granite after uniaxial recompression predamaged by high confining pressure cyclic loading based on acoustic emission. Eng. Fract. Mech. 266, 108414.
Yang, S.-Q., Ranjith, P., Huang, Y.-H., Yin, P.-F., Jing, H.-W., Gui, Y.-L., Yu, Q.-L., 2015. Experimental investigation on mechanical damage characteristics of sandstone under triaxial cyclic loading. Geophys. J. Int. 201 (2), 662–682.
Yang, S., Zhang, N., Feng, X., Kan, J., Pan, D., Qian, D., 2018. Experimental investigation of sandstone under cyclic loading: damage assessment using ultrasonic wave velocities and changes in elastic modulus. Shock Vib. 2018.
Ye, D., Wang, Z., 2001. A new approach to low-cycle fatigue damage based on exhaustion of static toughness and dissipation of cyclic plastic strain energy during fatigue. Int. J. Fatigue 23 (8), 679–687.
Yu, D., Liu, E., Sun, P., Xing, H., Zheng, Q., 2021. Dynamic mechanical properties and constitutive model for jointed mudstone samples subjected to cyclic loading. Eur. J. Environ. Civ. Eng. 1–27.
Zhang, J., Oueslati, A., Shen, W.Q., De Saxcé, G., 2019. Shakedown of porous material with Drucker-Prager dilatant matrix under general cyclic loadings. Compos. Struct. 220, 566–579.
Zhang, J., Shao, J., Zhu, Q., De Saxcé, G., 2022a. A bipotential-based macroscopic fatigue criterion of porous materials with a pressure-sensitive and non-associated plastic solid matrix and comparison with numerical simulation. Mech. Mater. 165, 104161.
Zhang, J., Shen, W., Oueslati, A., De Saxcé, G., 2017a. Shakedown of porous materials. Int. J. Plast. 95, 123–141.
Zhang, T., Xu, W., Wang, H., Wang, R., Yan, L., Shi, A., 2022b. Anisotropic mechanical characteristics and energy evolution of artificial columnar jointed rock masses subjected to multi-level cyclic loading. Int. J. Fatigue 107215.
Zhang, Y., You, Y., Moumni, Z., Anlas, G., Zhu, J., Zhang, W., 2017b. Experimental and theoretical investigation of the frequency effect on low cycle fatigue of shape memory alloys. Int. J. Plast. 90, 1–30.
Zhao, K., Ma, H., Liang, X., Li, X., Liu, Y., Cai, R., Ye, L., Yang, C., 2022. Damage evaluation of rock salt under multilevel cyclic loading with constant stress intervals using AE monitoring and CT scanning. J. Pet. Sci. Eng. 208, 109517.
Zhao, L.-Y., Zhu, Q.-Z., Shao, J.-F., 2018. A micro-mechanics based plastic damage model for quasi-brittle materials under a large range of compressive stress. Int. J. Plast. 100, 156–176.
Zhou, Y., Sheng, Q., Li, N., Fu, X., Zhang, Z., Gao, L., 2020. A constitutive model for rock materials subjected to triaxial cyclic compression. Mech. Mater. 144, 103341.
Zhou, S.-W., Xia, C.-C., Zhao, H.-B., Mei, S.-H., Zhou, Y., 2017. Statistical damage constitutive model for rocks subjected to cyclic stress and cyclic temperature. Acta Geophys. 65 (5), 893–906.
Zhu, Q., Shao, J.-F., 2015. A refined micromechanical damage-friction model with strength prediction for rock-like materials under compression. Int. J. Solids Struct. 60, 75–83.
Zhu, Q.-Z., Zhao, L.-Y., Liu, H.-X., Shao, J.-F., 2016a. Fast explicit integral algorithms with comparative studies for Shao-Zhu-Su rock rheological model. Chin. J. Rock Mech. Eng. 35 (02), 242–249.
Zhu, Q., Zhao, L., Shao, J., 2016b. Analytical and numerical analysis of frictional damage in quasi brittle materials. J. Mech. Phys. Solids 92, 137–163.
Zhu, Q., Zhou, C., Shao, J.-F., Kondo, D., 2010. A discrete thermodynamic approach for anisotropic plastic–damage modeling of cohesive-frictional geomaterials. Int. J. Numer. Anal. Methods Geomech. 34 (12), 1250–1270.